Vech, Daniel; Szego, K.; Opitz, A.; Kajdic, P.; Fraenz, M.; Kallio, Esa; Alho, Markku

Space weather effects on the bow shock, the magnetic barrier, and the ion composition boundary at Venus

Published in:
Journal of Geophysical Research: Space Physics

DOI:
10.1002/2014JA020782

Published: 01/01/2015

Document Version
Publisher's PDF, also known as Version of record

AGU PUBLICATIONS

JGR

Journal of Geophysical Research: Space Physics

RESEARCH ARTICLE

10.1002/2014JA020782

Key Points:

- Statistical study of the ICME-Venus interaction
- Analysis of solar wind and magnetic barrier conditions during ICME passages
- Decreased altitude of the nightside ionosphere during ICME passages

Correspondence to:
D. Vech,
vech.daniel@wigner.mta.hu

Citation:
Vech, D., K. Szego, A. Opitz, P. Kajdic, M. Fraenz, E. Kallio, and M. Alho (2015), Space weather effects on the bow shock, the magnetic barrier, and the ion composition boundary at Venus, *J. Geophys. Res. Space Physics*, *120*, 4613–4627, doi:10.1002/2014JA020782.

Received 31 OCT 2014
Accepted 16 MAY 2015
Accepted article online 20 MAY 2015
Published online 12 JUN 2015

Space weather effects on the bow shock, the magnetic barrier, and the ion composition boundary at Venus

D. Vech[1,2], K. Szego[1], A. Opitz[1,3], P. Kajdic[4], M. Fraenz[5], E. Kallio[6], and M. Alho[6]

[1]Department of Space Physics and Space Technologies, Wigner Research Centre for Physics, Budapest, Hungary, [2]Division of Space Technology, Department of Computer Science, Electrical and Space Engineering, Luleå University of Technology, Kiruna, Sweden, [3]European Space Research and Technology Center, European Space Agency, Noordwijk, Netherlands, [4]Instituto de Geofísica, Universidad Nacional Autónoma de México, Mexico City, Mexico, [5]Max-Planck-Institute for Solar System Research, Göttingen, Germany, [6]Department of Radio Science and Engineering, University of Aalto, Espoo, Finland

Abstract We present a statistical study on the interaction between interplanetary coronal mass ejections (ICMEs) and the induced magnetosphere of Venus when the peak magnetic field of the magnetic barrier was anomalously large (>65 nT). Based on the entire available Venus Express data set from April 2006 to October 2014, we selected 42 events and analyzed the solar wind parameters, the position of the bow shock, the size and plasma properties of the magnetic barrier, and the position of the ion composition boundary (ICB). It was found that the investigated ICMEs can be characterized with interplanetary shocks and unusually large tangential magnetic fields with respect to the Venus-Sun line. In most of the cases the position of the bow shock was not affected by the ICME. In a few cases the interaction between magnetic clouds and the induced magnetosphere of Venus was observed. During these events the small magnetosonic Mach numbers inside magnetic clouds caused the bow shock to appear at anomalously large distances from the planet. The positions of the upper and lower boundaries of the magnetic barrier were not affected by the ICMEs. The position of the ICB on the nightside was found closer to the planet during ICME passages which is attributed to the increased solar wind dynamic pressure.

1. Introduction

The induced planetary magnetosphere is the result of the interaction between the streaming solar wind plasma and an unmagnetized planetary body with an ionosphere acting as an obstacle. The upstream supersonic solar wind flow abruptly slows down ahead of the obstacle, and this process leads to the formation of a bow shock, which is a magnetohydrodynamic (MHD) discontinuity.

In the case of Venus, the size of the effective obstacle against the solar wind is determined by the altitude of the ionopause and the magnetic barrier. The magnetic barrier is the region of the induced magnetosphere in which the magnetic pressure dominates all other pressure contributions. The magnetic barrier forms in the dayside magnetosheath. It transfers the solar wind momentum to the ionosphere via increased magnetic pressure [*Zhang et al.*, 1991]. The upper boundary of the magnetic barrier is located at the altitude where the solar wind dynamic pressure is equal to the magnetic pressure in the induced magnetosphere [*Zhang et al.*, 2008a]. Here and later in the paper the solar wind dynamic pressure refers to the total dynamic pressure which is defined as ρv^2, where ρ denotes the solar wind mass density and v is the solar wind velocity. An additional boundary layer can be defined based on the plasma measurements. The ion composition boundary (ICB) is defined as the inner boundary of the magnetosheath, and it is characterized by significant heavy ion fluxes and a sudden decrease in the number density of the solar wind protons [*Martinecz et al.*, 2008].

The location of the Venusian bow shock is controlled by time-varying external conditions such as the magnitude and direction of the interplanetary magnetic field (IMF) and the velocity, density, and temperature of the solar wind. The position of the ICB is mainly controlled by the solar wind dynamic pressure [*Wei et al.*, 2012; *Angsmann et al.*, 2011].

The purpose of this study is to investigate the interaction between the plasma environment of Venus and interplanetary coronal mass ejections (ICMEs) when the magnetic field magnitude of the Venusian magnetic barrier is anomalously large. We analyze the ICMEs that cause these unusually high magnetic field intensities in the induced magnetosphere, and we discuss the plasma properties of the magnetic barrier, the position of the bow shock, and the ion composition boundary during these events.

ICMEs are large-scale plasma structures ejected from the Sun that drive the space weather conditions in the inner heliosphere. They cause drastic changes in the direction and magnitude of the IMF and the solar wind parameters. Their effect on the terrestrial planets is significant and is in the focus of the space physics community.

The effects of the ICMEs on the induced magnetosphere of Venus were discussed by several authors in recent works [e.g., *Luhmann et al*., 2008; *Zhang et al*., 2008b; *Edberg et al*., 2011]. It was found that ICMEs can largely modify the polarity of the induced magnetosphere, enhance the ion heating processes, and cause increased ion loss rate. According to the observations of *Zhang et al*. [2008b], based on a single case study of the Venus-ICME interaction, the magnetic barrier also showed unusual feature: the magnitude of the magnetic field in this region was over 90 nT during the passage of the ICME, which is nearly twofold increase compared to its average value.

The structure of a typical fast ICME consists of the magnetic cloud, the shock front, and a sheath region between them. The first indicator of the arrival of the fast ICME at the spacecraft is the ICME shock observation. The ICME shock is followed by the sheath region, which contains heated and shocked solar wind plasma. Often several hours after the arrival of the ICME-driven shock, the so-called magnetic cloud, which can be considered a substructure of the ICME, is detected [*Kilpua et al*., 2013]. Magnetic clouds were first observationally defined by *Burlaga et al*. [1981] as solar wind structures with higher than average magnetic field magnitudes, smooth large-scale rotations of the magnetic fields, and diminished proton temperatures. They are often associated with low proton densities [*Leamon et al*., 2002]. From statistical studies at the orbit of Earth, one third of the ICMEs show the signatures of a magnetic cloud [*Gosling*, 1990].

Anomalous positions of the Venusian bow shock were first observed by *Russell and Zhang* [1992] during times when the solar wind Mach number was low. A later study of the anomalous Venusian bow shock position was carried out by *Zhang et al*. [2008b], who focused on a single event. These authors reached the conclusion that distant bow shock crossings during the passage of ICMEs are due to the low bow shock magnetosonic Mach number during that time. The position of the ICB in tenuous solar wind (solar wind density below 0.2 cm^{-3}) was studied by *Wei et al*. [2012], and it was found that the ionosphere formed a teardrop shape in this case and its altitude increased both on the dayside and on the nightside. These observations were explained by the combined effect of enhanced source (transterminator flow) and reduced sink (ion loss into the interplanetary space) in tenuous solar wind. This study shows that the ion composition boundary is responsive to the solar wind dynamic pressure.

In the early age of the exploration of Venus, it was shown that the distance of the bow shock is very sensitive to the EUV flux from the Sun and that it correlates well with the solar cycle [*Slavin et al*., 1979]. During the solar minimum in 1976, the Venera 9/10 spacecraft detected the bow shock at an average of 2.14 Venus radii (R_V) in the terminator plane, while 3 years later near the solar maximum, the Pioneer Venus Orbiter detected it at an average of 2.4 R_V [*Russell et al*., 1988]. The reasoning for this dependence is that during the solar maximum, the higher EUV flux heats the atmosphere and increases the altitude of the ionopause, which in turn creates a larger obstacle leading to the observed changes in the bow shock position [*Russell et al*., 1988].

The dependence of the position of the bow shock on the direction of the IMF is discussed by *Alexander and Russel* [1985]. According to their findings, the bow shock is closer to the planet when the direction of the IMF and the solar wind velocity vector are parallel or antiparallel. On the other hand, when these vectors are perpendicular, the shock is farther away from the planet. *Zhang et al*. [2009] offered the following explanation for this: during the times when the interplanetary magnetic field is nearly aligned with the solar wind flow, the magnetic barrier disappears and the size of the obstacle decreases, thus causing the bow shock to occur closer to the planet. In a recent study, *Chai et al*. [2014] found that the bow shock distance highly depends on the magnitude of the IMF and its tangential component (B_{tan}) with respect to the Venus-Sun line. The study showed that the bow shock distance at the terminator increases with increasing IMF magnitude and that there is a linear relationship between the B_{tan} and the distance of the bow shock.

From the MHD point of view, the bow shock is a fast magnetosonic wave propagating toward the Sun and away from the planet in the solar wind reference frame. The position of the bow shock highly depends on the ratio of the solar wind velocity and magnetosonic velocity. The importance of the magnetosonic Mach number (M_{ms}) is discussed by several authors [e.g., *Farris and Russell*, 1994; *Edberg et al.*, 2010]. The average M_{ms} at the nose of the Venusian bow shock is approximately 5 [*Russell et al.*, 2006]. According to *Edberg et al.* [2010], the distance of the Venusian bow shock from the planet is inversely proportional to the upstream magnetosonic Mach number.

The solar wind dynamic pressure on the Venusian bow shock has also been investigated by several authors [e.g., *Martinecz et al.*, 2008; *Edberg et al.*, 2010; *Russell et al.*, 1988; *Zhang et al.*, 2004]. It was concluded that the solar wind dynamic pressure plays only a minor role in the position of the bow shock at Venus. *Martinecz et al.* [2008] even stated that during solar minimum, the bow shock is insensitive to the solar wind dynamic pressure.

The paper is organized as follows: in section 2 we summarize the instrumentation of Venus Express, STEREO, and Solar Heliospheric Observatory (SOHO) spacecraft. In section 3, the event selection method is discussed. In section 4 we present one of the analyzed events in details. Section 5 presents the list of the investigated ICMEs. Sections 5.1, 5.2, 5.3, and 5.4 focus on the statistical analysis of these 42 events, where we discuss the solar wind parameters, the position of the bow shock, the properties of the magnetic barrier, and the position of the ion composition boundary during ICME passages, respectively. Finally, we present the discussion along with our conclusions in sections 6 and 7.

2. Instrumentation

We used the in situ observations made by the Venus Express spacecraft in order to study in detail the plasma environment near the planet. The Venus Express (VEX) spacecraft is the first European mission sent to Venus [*Svedhem et al.*, 2007; *Titov et al.*, 2006]. It was launched on 9 November 2005 and reached Venus on 11 April 2006. VEX made measurements from an elliptic polar orbit with 24 h period. The distance of the apocenter was 66,000 km, and the pericenter altitude was maintained in the range of 250–350 km. During the aerobraking campaign between 17 May and 12 June 2014, the pericenter altitude was allowed to decrease to 132 km, and the orbital period was reduced to 22.5 h [*Svedhem*, 2014]. VEX carried seven instruments on board. Here we use the magnetic field measurements from the Magnetometer (MAG) and the plasma data from the Analyzer of Space Plasmas and Energetic Atoms version 4 (ASPERA-4) instrument package.

The ASPERA-4 includes four detectors: the Ion Mass Analyzer (IMA), the Neutral Particle Imager, the Neutral Particle Detector, and the Electron Spectrometer (ELS) [*Barabash et al.*, 2007]. In our study, only data from the ELS electron and IMA ion instruments were used.

The ELS experiment detects electrons with energies in the range of 0.01–15 keV/charge, and its energy resolution ($\Delta E/E$) is 0.07. Normally, ELS measures only a two-dimensional cut of the distribution function, but since the electron distribution is usually gyrotropic, the two-dimensional cut allows an extrapolation to the full distribution of the density and temperature. We used the electron moments described by *Fraenz et al.* [2006] for the electron temperature data, which was an input parameter for the magnetosonic Mach number. The magnetosonic Mach number was derived from the following equation:

$$M_{\mathrm{ms}} = \frac{v_{\mathrm{sw}}}{\sqrt{V_A^2 + V_S^2}} \tag{1}$$

Here v_{sw} is the solar wind proton velocity, $V_A = B/(\rho\mu_0)^{1/2}$ is the Alfvén speed, and $V_S = (\Upsilon p/\rho)^{1/2}$ is the sound speed. The B denotes the magnetic field; ρ the solar wind mass density; μ_0 the permeability of vacuum; $\Upsilon = 5/3$ is the ratio of specific heats; and $p = n\ k_B\ (T_e + T_i)$ is the thermal pressure of the solar wind, where n denotes the density of the solar wind, k_B the Boltzmann constant, and T_e and T_i are the electron and ion temperatures, respectively. For the dynamic and thermal pressure calibration it was assumed that the ratio of the alpha particle and proton number density is 0.04 [*Edberg et al.*, 2010].

The IMA experiment is capable of detecting ions with energies in the range of 0.01–36 keV/charge with the energy resolution of $\Delta E/E = 0.07$. The time resolution is 192 s, and the field of view is 90° × 360° [*Barabash et al.*, 2007]. Here we use the proton temperature, proton density, the energy spectrograms for heavy ions and protons, and the derived proton velocity (vector components).

Table 1. Distribution of the Peak Values of the Magnetic Field of the Magnetic Barrier Between April 2006 and October 2014[a]

Peak of the Magnetic Field of the Magnetic Barrier (nT)	2006 (209)	2007 (344)	2008 (331)	2009 (283)	2010 (247)	2011 (304)	2012 (318)	2013 (338)	2014 (238)
15–25	1.9% (4)	3.7% (13)	7.8% (26)	9.8% (28)	5.6% (14)	3.2% (10)	8.4% (27)	5.9% (20)	3.3% (8)
25–35	19.6% (41)	23.2% (80)	31.4% (104)	39.9% (113)	25.9% (64)	20.3% (62)	24.2% (77)	18% (61)	20.1% (48)
35–45	28.2% (59)	34.8% (120)	33.2% (110)	32.5% (92)	35.6% (88)	32.5% (99)	33.3% (106)	29.8% (101)	36.1% (86)
45–55	29.6% (62)	24.7% (85)	19.0% (63)	12.7% (36)	19.0% (47)	23.3% (71)	16.6% (53)	21.3% (72)	20.1% (48)
55–65	15.3% (32)	6.9% (24)	7.2% (24)	2.4% (7)	8.0% (20)	10.5% (32)	8.8% (28)	13.9% (47)	12.6% (30)
65–75	**2.3% (5)**	**3.4% (12)**	**1.2% (4)**	**1.7% (5)**	**2.8% (7)**	**5.5% (17)**	**3.7% (12)**	**2.9% (10)**	**5.0% (12)**
75–85	**1.9% (4)**	**1.1% (4)**		**0.3% (1)**	**1.6% (4)**	**1.9% (6)**	**1.2% (4)**	**0.8% (3)**	**1.6% (4)**
85–95	**0.9% (2)**	**1.4% (5)**		**0.3% (1)**	**1.2% (3)**	**0.6% (2)**	**1.5% (5)**	**0.2% (1)**	**0.8% (2)**
95–105		**0.2% (1)**						**0.5% (2)**	
105–115						**0.6% (2)**		**0.5% (2)**	
115–125								**0.2% (1)**	
…									
135–145						**0.6% (2)**	**1.3% (1)**		
…									
225–235						**0.3% (1)**			

[a]The first column contains the bins of the peak intensity of the magnetic field in the magnetic barrier, while columns 2–10 contain the absolute (number of events) and relative (in %) occurrence for 9 years from 2006 to 2014. In this study we are interested in the events with higher than 65 nT peak value (bins in bold).

The MAG experiment is a triaxial fluxgate magnetometer made of two sensors which are operating continuously. The standard operation mode of both sensors is 1 Hz. One hour before the pericenter, the instrument is switched to fast mode which enables 32 Hz sampling rate. This operation mode is switched off 1 h after the pericenter. The instrument is set to burst mode of 128 Hz, 1 min before pericenter, and it lasts for 2 min [*Zhang et al.*, 2006].

In addition to the in situ VEX measurements, we use the coronagraph images of the Solar Terrestrial Relations Observatory (STEREO) A and B and the Solar Heliospheric Observatory (SOHO) spacecraft to confirm that the observed changes in the plasma and magnetic field parameters at the Venus orbit are associated with ICME passages. The STEREO spacecraft were launched in 2006 and are orbiting the Sun at approximately 1 AU in opposite directions. Since then, they have been providing great detailed observations of solar flares, CMEs, ICMEs, corotating interaction regions, and solar wind parameters at two vantage points [*Kaiser et al.*, 2008]. The SOHO spacecraft was placed into the L1 Sun-Earth Lagrangian point in 1995 and has continued to reliably observe the solar atmosphere since its insertion [*Domingo and Poland*, 1988].

3. Event Selection

For the event selection the entire available VEX data set was used from 30 April 2006 to 12 October 2014. The peak magnetic field of the magnetic barrier was obtained for each orbit. The magnetic barrier was identified in the dayside magnetosheath as the region with the highest magnetic field. Table 1 contains the distribution of the peak magnetic field values of the magnetic barrier for every possible orbit during the entire time period. Due to the gaps in the MAG data it was not possible to consider all orbits. Nearly 2600 orbits were investigated, and it was found that the average of the peak values is approximately 42 nT. We were interested in the cases when the peak of the magnetic field was significantly higher than this value. For this purpose we selected the events with peak values higher than 65 nT, resulting in the identification of 152 events of interest (highlighted bins in Table 1).

Further investigation was required to confirm that the anomalous magnetic field intensities are due to ICMEs and to distinguish them from other space weather phenomena.

We used increase in the IMF which is followed by increase in the solar wind proton velocity and density as identification criteria in the in situ data [*Edberg et al.*, 2011]. For the final confirmation of the events, the coronagraph images of the STEREO A and B and the SOHO spacecraft were also used. We searched for CMEs that propagate into the correct direction near the ecliptic plane and lift off 30–50 h before the in situ observations because they can confirm that the changes seen in the VEX data are due to ICME passages.

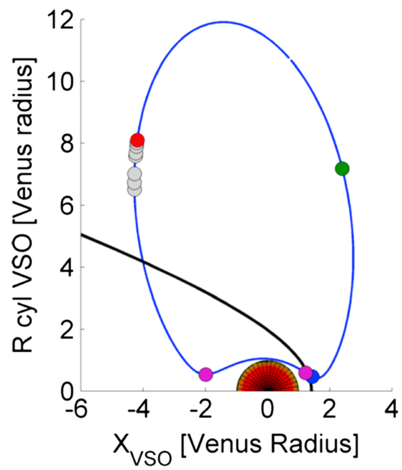

Figure 1. Orbit geometry of VEX on 5 November 2011. The black line shows the estimated bow shock position based on *Martinecz et al.* [2009], and the blue line is the orbit of VEX. The colored dots have the following meaning: green dot: detection the arrival of the interplanetary shock; blue and red dots: inbound and last outbound bow shock crossings, respectively; purple dots: inbound and outbound ICB crossings; and gray dots: locations of the eight multiple bow shock crossings at the flank before the last outbound crossing (red dot).

Out of the 152 events with high peak field, 42 could be clearly related to ICME passages. In the following, we analyze only those 42 events.

4. An Example Case: ICME Passage at Venus on 5–6 November 2011

An example of the interaction of the ICME and the induced magnetosphere of Venus is presented in Figures 1–3, where the ICME passage on 5–6 November 2011 will be analyzed. Here we show the 5 November 2011 event. Figure 1 shows the orbit geometry of VEX during this event. The spacecraft orbit is marked with a blue line, while the black lines show the estimated position of the nominal bow shock based on the fitted paraboloid by *Martinecz et al.* [2009] with the following parameters: eccentricity $\varepsilon = 1.056$, semilatus rectum $L = 1.303\,R_V$, and focus point located at (x, y, and z) = (0.788, 0, and 0) R_V. Figure 1 is presented in the Venus Solar Orbit (VSO) coordinates, where the X_{VSO} axis lies on the Sun-Venus line and points toward the Sun, the Z_{VSO} axis is perpendicular to the orbital plane of the planet pointing toward the ecliptic north, and the Y_{VSO} axis completes the right-hand triad pointing approximately in the direction opposite to the Venus orbital motion. In Figure 1 we use the cylindrical coordinate system with X_{VSO} on the horizontal axis, and the vertical axis is the distance from the X_{VSO} which is calculated as $(Z_{VSO}{}^2 + Y_{VSO}{}^2)^{1/2}$. In this case the orbit plane of VEX was nearly parallel to the X_{VSO}-Z_{VSO} plane, and therefore, the nose and the flank of the bow shock were both surveyed. In Figure 1, the colored dots have the following meaning: green dot: detection of the arrival of the interplanetary shock; blue and red dots: inbound and last outbound bow shock crossings, respectively; purple dots: inbound and outbound ICB crossings; and gray dots: locations of the eight multiple bow shock crossings at the flank before the last outbound crossing (red dot).

In Figure 2 the magnetic field data on 5 and 6 November 2011 are presented. The arrival of the ICME-driven shock (vertical green line) was observed on 5 November 2011 at 03:30 UT, and it can be recognized due to sudden increase of the IMF magnitude. It was distinguished from the bow shock based on the solar wind proton velocity measurements: at the interplanetary shock the velocity suddenly increased, while at the Venus bow shock the velocity dropped. VEX observed an inbound bow shock crossing on the day of the ICME arrival at 07:00 UT. The peak of magnetic field intensity in the magnetic barrier at this time reached 230 nT.

The second vertical red line at 12:30 UT on 5 November denotes the final outbound bow shock crossing after eight alternating inbound and outbound crossings. These encounters are marked by small vertical lines in Figure 2. During these bow shock movements the bow shock distance was increased and unfortunately located at a position where the ELS and IMA sensors of the ASPERA-4 experiment did not provide data even though the VEX spacecraft crossed this region. Therefore, the encounters were identified only based on spikes seen in the magnetic field data. During the following orbit on 6 November, the two vertical red lines at 07:00 UT and 10:00 UT represent inbound and outbound bow shock crossings, respectively. We observe based on the magnetic field data on 5 and 6 November 2011 that the elapsed time between the first inbound and last outbound bow shock crossings is significantly longer on 5 November 2011 (4.5 h) compared to the following day with quiet solar wind conditions (3 h). This is due to the increased bow shock distance on 5 November 2011, which is discussed in details in the following sections. It can be seen that after the last outbound bow shock crossing, the magnitude of the IMF decreased gradually and it reached its near-average

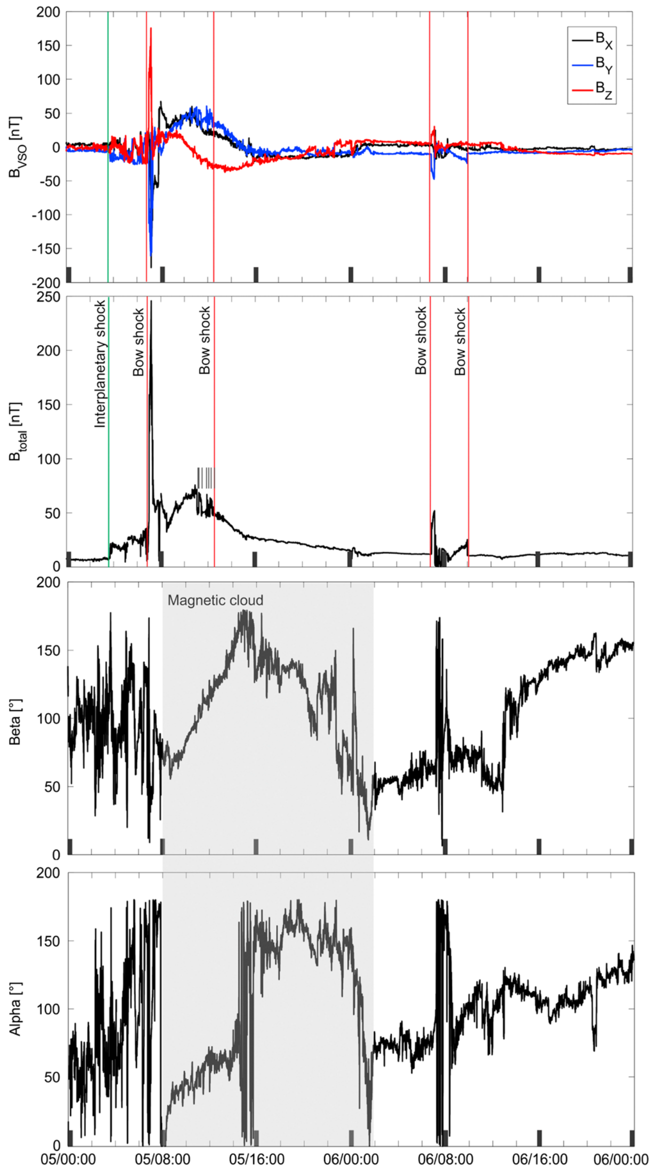

Figure 2. The VEX MAG data between 5 and 6 November 2011. (first panel) The magnetic field is presented in the Venus Solar Orbit (VSO) coordinate system. (third and fourth panels) The α and β angles of the magnetic field (described in the text) are shown in the VSO coordinate system.

value on 6 November 02:00 UT. On this day the peak B value of the magnetic barrier was near average (approximately 50 nT). Figures 2c and 2d show the $\alpha = \mathrm{acos}\left(\frac{B_x}{\sqrt{B_x^2+B_y^2}}\right)$ and $\beta = \mathrm{acos}\left(\frac{B_z}{B_{\mathrm{total}}}\right)$ angles of the magnetic field in the VSO coordinate system. The analysis of these angles can be used to identify magnetic structures including magnetic clouds since the rotation of the magnetic field can be displayed well with these angles [*Lepping et al.*, 2005]. During the period shaded in gray (from approximately 08:30 UT 5 November to 01:00 UT 6 November), the magnetic field displays smooth rotations. The observed changes of these angles and the magnetic field components are typical features of the passage of magnetic clouds [*Lepping et al.*, 2005]. The gray area overlaps with the VEX observations in the Venusian magnetotail, which means that the signatures of the magnetic cloud passage were observed inside the induced magnetosphere of this planet as well as after the multiple bow shock crossings on 5 November. We note that the observed pattern of the magnetic field is very unusual and the magnetic cloud-induced magnetosphere interaction was observed in only 6 out of 42 investigated ICMEs.

Figure 3 shows the measurements of the ASPERA-4 and MAG instruments near the ion composition boundary. In Figure 3a, we show the observations during the passage of the ICME which arrived at Venus on 5 November 2011, while in Figure 3b, the measurements on a quiet day (2 days after the ICME) are presented. For both days we show the heavy ion energy spectrogram, the proton energy spectrogram, and the magnetic field measurements. On 5 November 2011, VEX crossed the bow shock at 07:00 UT. After passing through the bow shock VEX entered the magnetosheath, which is marked with light blue shading. At 7:06 UT, the spacecraft reached the outer boundary of the magnetic barrier, which is the altitude where the external solar wind dynamic pressure is equal to the magnetic pressure in the induced magnetosphere [*Zhang et al.*, 2008a]. The time interval in which the magnetic pressure dominates over all other pressure contributions is marked with dark gray in Figure 3a (bottom) and is identified as the magnetic barrier. On 5 November 2011, VEX crossed the ion composition boundary at 07:10 UT which can be recognized as the first appearance of significant heavy ion fluxes. This is denoted with the first vertical red line. The outbound crossing was observed at 07:47 UT and was associated with

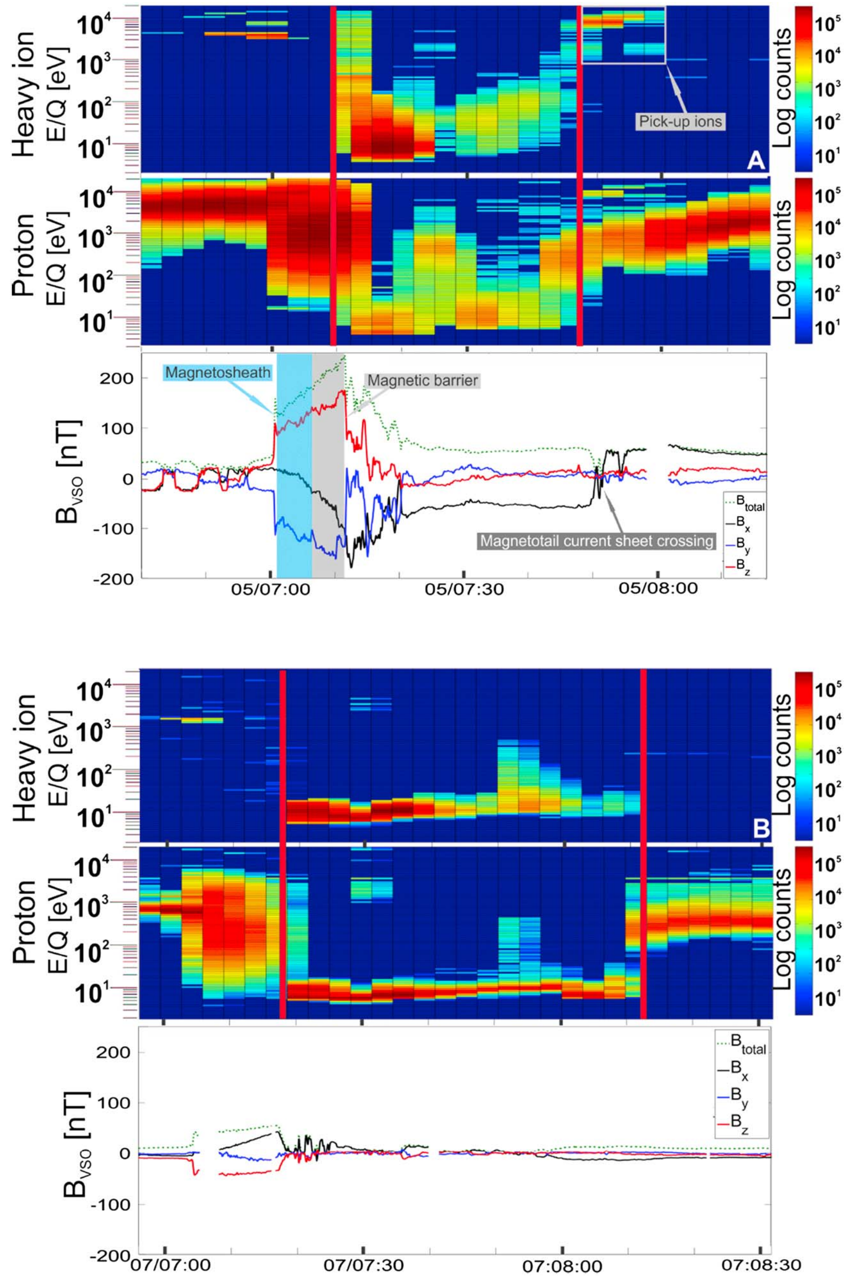

Figure 3. Plasma and magnetic field data near the ion composition boundary during the passage of the interplanetary coronal mass ejection on (a) 5 November 2011 and on a quiet day on (b) 7 November 2011. In Figures 3a and 3b, the top plots show the heavy ion energy spectrogram, and the middle plots show the proton energy spectrogram. In the bottom plots, the magnetic field components are presented in VSO coordinates. The ICB crossings are denoted with red vertical lines. In the panels of the heavy ion and proton spectra, the *Y* axis represents the energy/charge ratio, and the colors are related to the number of the counts in the energy bins.

the disappearance of the major heavy ion flux (second vertical red line). After the outbound crossing, an ion population with very high energies (10^4 eV) was detected at 07:50 UT. At the same time, the B_X component of the magnetic field (Figure 3a, bottom) changed sign abruptly which is the signature of the magnetotail current sheet crossing [*Fedorov et al.*, 2008]. Under normal conditions the magnetotail current sheet is filled by heavy ions with energies in the range of 500–1000 eV [*Fedorov et al.*, 2008]. During the passage of the ICME the energies of the heavy ions in this region increased with an order of magnitude. We identified the heavy ions in this region as pickup ions [*McEnulty et al.*, 2010].

Table 2. The Dates of Arrival for the 42 ICMEs Analyzed in This Study and the Observation of Interplanetary Shocks and Magnetic Cloud Passages

Event Number	ICME Arrival at Venus	Observation of Interplanetary Shock	Interaction Between the Magnetic Cloud and the Induced Magnetosphere of Venus
1	5 July 2006		
2	11 September 2006	✓	✓
3	19 May 2007		
4	25 June 2007	✓	
5	13 July 2007		
6	18 November 2007		
7	9 February 2008		
8	3 October 2009		
9	17 October 2009		
10	3 March 2010	✓	
11	18 March 2010	✓	
12	10 August 2010	✓	
13	20 August 2010	✓	
14	9 October 2010	✓	
15	19 February 2011	✓	
16	11 April 2011	✓	
17	21 April 2011	✓	
18	21 May 2011	✓	
19	27 May 2011	✓	
20	28 July 2011	✓	
21	16 October 2011	✓	✓
22	1 November 2011	✓	
23	5 November 2011	✓	✓
24	18 November 2011	✓	
25	19 November 2011	✓	✓
26	2 March 2012	✓	
27	12 May 2012	✓	
28	30 May 2012	✓	
29	16 June 2012	✓	✓
30	8 July 2012	✓	
31	11 July 2012	✓	
32	19 July 2012	✓	
33	30 July 2012	✓	
34	7 March 2013	✓	
35	25 September 2013	✓	
36	5 October 2013	✓	
37	28 October 2013	✓	✓
38	20 February 2014	✓	
39	9 May 2014	✓	
40	10 May 2014	✓	
41	24 September 2014	✓	
42	26 September 2014	✓	

For the quiet day (Figure 3b) the inbound and outbound ICB crossings happened at 07:17 and 08:13 UT, respectively, and are again denoted with vertical red lines. We observe that the elapsed time between the inbound and outbound ICB crossings during the passage of the ICME on 5 November 2011 was significantly shorter (37 min) than on the quiet day on 7 November 2011 (56 min).

5. Statistical Analysis of All ICME Passages During VEX Observations

Based on the selection method described in section 3, we found 42 events between April 2006 and October 2014 that could be clearly related to ICME passages. The dates when these ICMEs reached Venus are summarized in Table 2. In the third and fourth columns, the observation of interplanetary shocks and the interaction between the magnetic cloud and the induced magnetosphere of Venus are denoted with ticks.

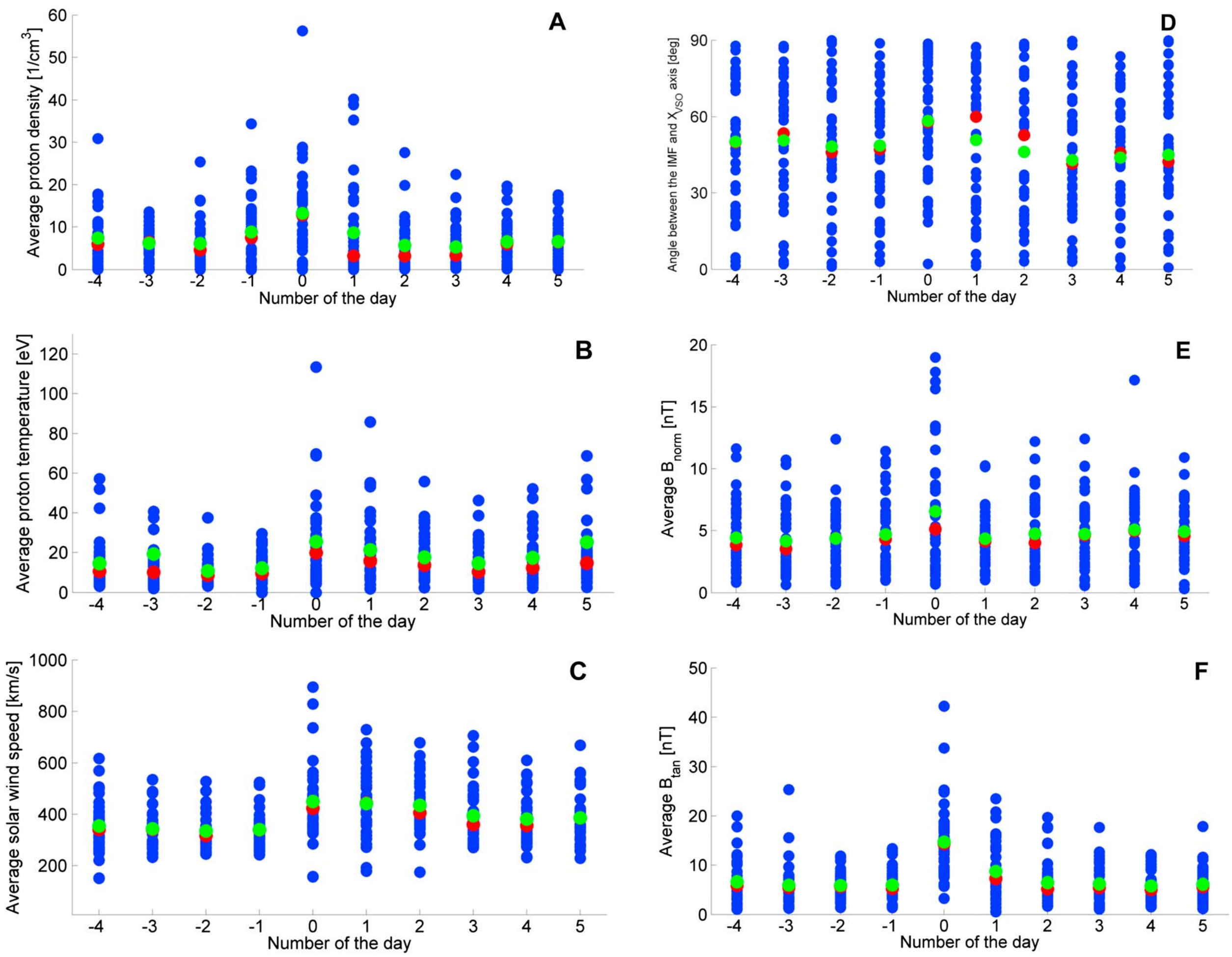

Figure 4. Twenty minute average of the solar wind parameters before inbound bow shock crossing in the analyzed 42 cases. Ten day periods are presented which are centered on the day the ICME arrived at Venus (day 0). The data points on each day are marked with blue circles, while the median and average values of each bin (each day) are in green and red, respectively. The (a) proton density, (b) proton temperature, (c) solar wind proton velocity, (d) angle between the IMF and the X_{VSO} axis, (e) normal, and (f) tangential components of the IMF are presented. The magnetic field measurements (Figures 4d–4f) are based on the VSO coordinate system.

5.1. Solar Wind Parameters

In this section we present a statistical analysis of the solar wind proton density, temperature, velocity, and IMF for the 42 ICME passages.

In Figure 4 the observed solar wind parameters are shown for the 42 investigated cases. Twenty minute average was considered before inbound bow shock crossings on each day. The data for 10 consecutive days are presented. The days are marked with numbers from -4 to 5. The number 0 represents the day of the ICME arrival at Venus. The data on day 0 were always measured inside the arriving ICME. The data points on each day are marked with blue circles, while the median and average values of each bin are in green and red, respectively. In Figure 4e, the B_{norm} is equivalent to the X component of the magnetic field in the VSO system. In order to make these magnetic field measurements easily comparable, the positive and negative signs are omitted and the absolute values are presented. The tangential component in Figure 4f was derived with the following formula: $B_{\tan} = \sqrt{B_y^2 + B_z^2}$.

According to Figures 4a–4c, the density of the solar wind was enhanced slightly while the temperature of protons increased significantly on day 0 compared to the previous days. In most of the cases, the solar wind velocity increased on day 0 and remained enhanced on day 1 as well. The magnetic fields in

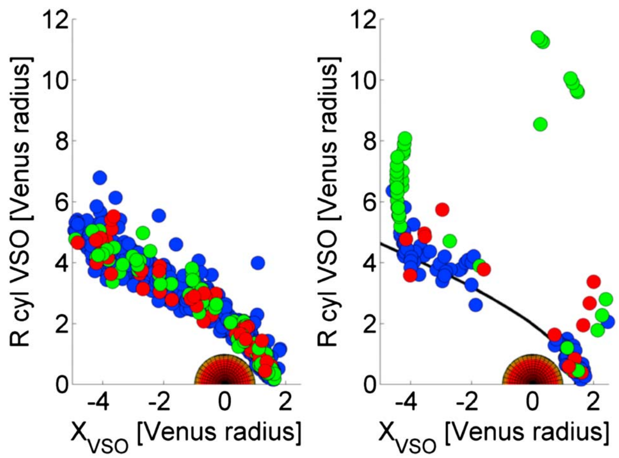

Figure 5. Locations of the bow shock crossing for all the 42 investigated events. The green marks show the bow shock crossings (including the multiple bow shock crossings as well) on the day when the ICME arrived at Venus, the red dots represent the bow shock location during the following day, and the rest of the days are marked with blue dots. (left) Thirty-six cases when the interaction between the magnetic cloud and the induced magnetosphere was not observed and (right) six cases when the signature of the passing magnetic cloud was detected.

Figures 4d–4f show that the direction of the IMF with respect to the X_{VSO} axis changed and was closest to 90° during the ICME. In Figure 4e, the normal component of the IMF was higher than average on day 0 in several cases, but the average and median values show that on a statistical basis, the increase of this magnetic field component was not significant. In Figure 4f, the tangential component of the IMF is presented, and it can be seen that average and median values on day 0 nearly doubled compared to the other days. We also note that the B_{tan} remained unusually high even on day 1 in most of the cases.

5.2. Bow Shock Positions

The position of the Venusian bow shock was studied during the ICME passages. The location of the bow shock was identified with the use of the MAG, ELS, and IMA data. In a few cases the bow shock distance was increased to altitudes where the ASPERA-4 and ELS instruments did not provide data. In these cases we rely only on MAG magnetic field measurements. We have sorted the events into two groups by differentiating cases where there was no magnetic cloud (only ICME shock and sheath) observed by VEX (36 cases) and cases where there was a clear signature of a magnetic cloud passage at Venus (6 cases). During the 36 ICME sheath cases (Figure 5, left), the bow shock remained unchanged, while in the six magnetic cloud events (Figure 5, right), we observed a largely expanded bow shock even at distances above 10 R_V. We also note that in some cases the bow shock position remained anomalous on day 1 as well.

5.3. Properties of the Magnetic Barrier

In this section we discuss the observations of the magnetic barrier during ICME passages. The magnetic field of the magnetic barrier was our event selection criterion (field strength greater than 65 nT); therefore, we focus here on other parameters: the position of the upper boundary and the plasma parameters of this region.

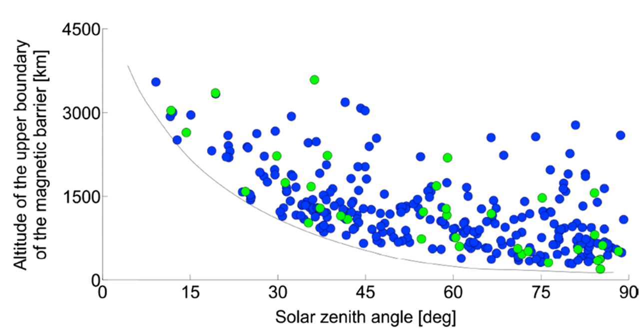

Figure 6. Position of the upper boundary of the magnetic barrier as a function of the solar zenith angle for the 42 events. The position on the day when the ICME arrived at Venus is denoted with green circles, while the blue ones represent the rest of the days. The black line shows the boundary below which VEX did not enter.

In Figure 6, we present the position of the upper boundary of the magnetic barrier for the 42 events. The Y axis shows the altitude measured from the surface of Venus, while the X axis shows the solar zenith angle. The green dots show the position of the upper boundary on day 0, while the blue ones show positions for the other days. The position of the upper boundary was determined as the altitude where the solar wind dynamic pressure and the magnetic pressure were equal

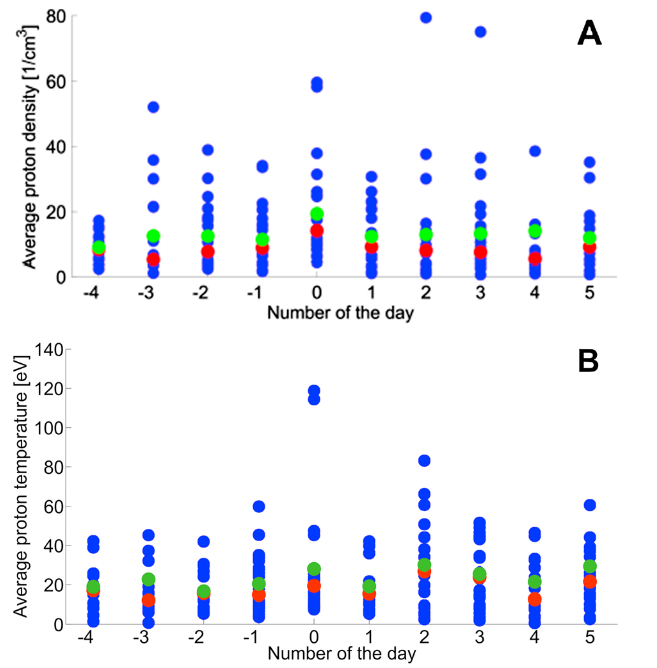

Figure 7. (a) Average proton density and (b) proton temperature of the magnetic barrier for the 42 events. The ICME arrived at Venus on day 0. The data points on each day are marked with blue. The red dots show the median values, while the green dots show the average values of the bins.

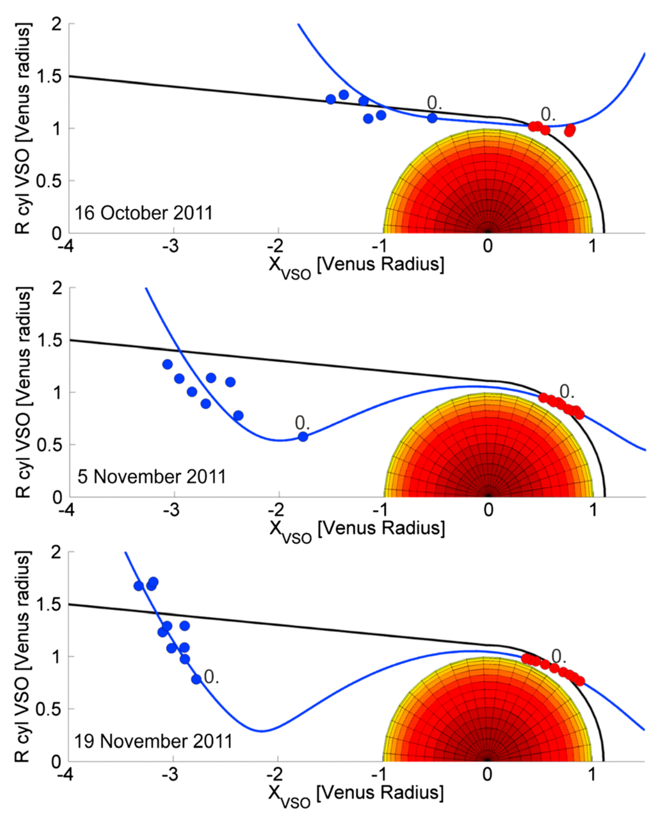

Figure 8. Three examples from the investigated events to show the ICB variations during ICME passages. Note that the ASPERA-4 data were not always available; therefore, there can be less than 10 inbound and outbound crossings presented here.

[*Zhang et al.*, 2008a]. For this purpose we calculated the magnetic and dynamic pressure for each location along the VEX orbit and selected the point where they were equal.

Although there is some scattering in the data, it can be seen that the position of the upper boundary was not anomalously close or far from its nominal position during the ICME passages and we cannot see such outliers like in the case of the bow shock crossings in Figure 5.

Figure 7 shows the average proton density (Figure 7a) and proton temperature (Figure 7b) of the magnetic barrier for the 42 investigated cases. These average values are given for the 10 consecutive days around the ICME arrivals (as in Figure 4) and are calculated from the plasma measurements made between the upper boundary of the magnetic barrier and the ICB crossings. In Figure 7a, it can be seen that the proton density significantly increased on day 0. The proton temperature data in Figure 7b show that although there were some outliers, the median and average values of the proton temperature were not enhanced during the ICME passages.

5.4. Position of the Ion Composition Boundary

In this section we study the position of the ICB as a function of the space weather at Venus. We show three examples of observed ICB positions from our event list (Table 1) in Figure 8, where the black line shows the average position of the nominal ICB based on the fitted model by *Martinecz et al.* [2009]. The following parameters were used for the fitting: the dayside ($X_{VSO} > 0$) is fitted with a circle ($r_{circle} = 1.109\,R_V$) and the nightside ($X_{VSO} < 0$) is approximated with

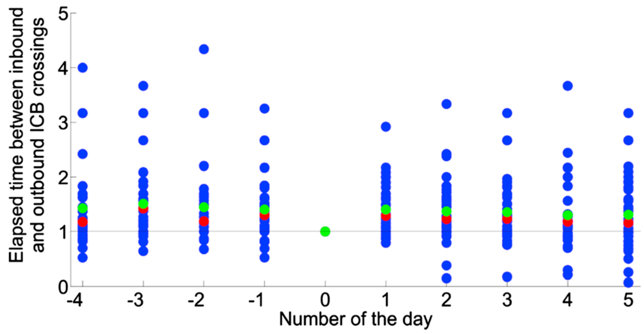

Figure 9. The ratio of the elapsed time between inbound and outbound ICB crossings on quiet days and day 0. The data points on each day are marked with blue. The red dots show the median, while the green ones show the average values of the bins.

$(Y_{VSO}+Z_{VSO})^{1/2}=k\cdot X_{VSO}+d$, where $k=-0.097$ and $d=1.109\,R_V$. In Figure 8, 10 day intervals are presented, and the red and blue dots show the inbound and outbound ICB crossings, respectively. The blue line shows the VEX orbit on the day when the ICME arrived at Venus. The VEX orbit plane changes constantly; therefore, during the days before and after the ICME passage, VEX crossed the ICB at different locations. This is the reason not all the dots are on the blue line. The panels show that on the dayside, the location of the ICB remained unchanged during the ICME passage. On the nightside the altitude of the ICB decreased significantly on day 0. These cases are considered to be anomalous because they significantly deviate from the average ICB distances on the nightside in the 10 consecutive day intervals, being usually the closest ICB crossings to Venus in those periods.

We investigate the elapsed time between the inbound and outbound ICB crossings for the 42 events in Figure 9. This figure has the same format as Figures 4 and 7. The orbit plane of VEX was different in each of the cases, and the elapsed time between the inbound and outbound ICB crossings was influenced by this factor. In order to make the different orbits easily comparable, the following normalization was used: the elapsed time between the inbound and outbound ICB crossings in the 10 day intervals were divided by the elapsed time on day 0 when the ICME arrived. In this way it was possible to analyze how the elapsed time changed during the ICME passages as compared to the other quiet days.

Figure 9 shows that on day 0, i.e., when the ICME arrived, the elapsed time between the inbound and outbound ICB crossings decreased as compared to the other days. On average, VEX spent nearly 33% less time in the ionosphere on day 0 than on the quiet days when no ICME was observed.

6. Discussion

In this study we presented a statistical analysis based on the peak magnetic field magnitude of the magnetic barrier. We were interested in the cases when the magnetic field was anomalously large (above 65 nT) in the magnetic barrier. Using the entire available VEX data set (approximately 2600 orbits), we found that 152 events met this requirement. After careful analysis, we selected 42 of them that could be associated with the passage of ICMEs. We analyzed the solar wind parameters, the position of the bow shock, the position of the ICB, and the size and plasma parameters of the magnetic barrier during these events.

We investigated the effects of 42 ICMEs and found that 36 out of them (83%) drove interplanetary shocks. In the cases of the ICMEs that drove interplanetary shocks, the peak magnetic field magnitude of the magnetic barrier was approximately 234 nT, while during the nonshock events, it was only approximately 91 nT. All the ICMEs that did not drive interplanetary shocks were observed during the period of 2006–2009. *Jian et al.* [2013] surveyed the ICME parameters in the raising phase of the recent solar cycle based on the STEREO spacecraft data. The ICME shock rate was low during the period of 2006–2009 (2006: 60%, 2007: 30%, 2008: 0%, and 2009: 30%), while in 2010 and 2011, it reached 50%.

The investigation of the solar wind parameters in front of the inbound bow shock crossings at Venus showed that both the solar wind proton density and the proton temperature increased significantly during the ICME passages. The solar wind velocity was enhanced on day 0 and remained higher than usual on day 1 as well. The sudden increase of the solar wind dynamic pressure due to the interplanetary shock caused a pressure pulse that interacted with the plasma environment of Venus.

Table 3. The Magnetosonic Mach Numbers for the Six Events When the Interaction Between the Plasma Environment of Venus and the Magnetic Cloud Was Observed[a]

	Magnetosonic Mach Number		
Date	Undisturbed Solar Wind	ICME Sheath Region	Magnetic Cloud
11 September 2006	4.41	3.91	1.12
16 October 2011	3.32	5.18	1.19
5 November 2011	4.63	3.87	1.21
19 November 2011	3.73	4.27	1.24
16 June 2012	3.25	3.43	1.37
28 October 2013	3.01	3.68	1.41

[a]The M_{ms} values before the arrival of the ICME, in the ICME sheath region, and in the magnetic cloud are presented.

The bow shock position was discussed separately depending on the observation of magnetic clouds. We found that the unusually large bow shock distances are due to the magnetic cloud passages. These are considered to be rare events since only 6 of the 42 cases showed the signature of this interaction. The magnetosonic Mach numbers (M_{ms}) for these six events are shown in Table 3. This parameter is very important since the position of the bow shock is primarily the function of the upstream magnetosonic Mach number. The bow shock distance is inversely proportional to the upstream M_{ms} [*Edberg et al*., 2010]. The M_{ms} values of the undisturbed solar wind, the ICME sheath region, and the magnetic cloud are presented. It can be seen that the M_{ms} inside the magnetic clouds always approaches unity, which then explains why during magnetic cloud passages the bow shock was always found at large distances from the planet. Based on our observations we can say that the M_{ms} has the dominant influence on the location of the Venusian bow shock since the M_{ms} has lowest values during the magnetic cloud passage.

The observed size and the plasma parameters of the magnetic barrier were also analyzed. The thickness of the barrier did not change during the ICME passages. Neither the position of its upper boundary nor its lower boundary (the dayside ICB) was affected by the ICMEs. This finding implies that the anomalously large magnetic field in this region is due to the increased pileup of the IMF magnetic field lines and not due to the compression of the barrier during the ICME passage. The solar wind proton density increased at the barrier, which can be explained with the increased density of the plasma in the ICME (e.g., more protons entered the magnetic barrier). Since the solar wind proton temperature was enhanced before inbound bow shock crossings, we expected that the proton temperature is increased in the barrier as well. However, the proton temperature at the barrier was average during the ICME passages. This implies that after passing through the bow shock, the cooling of the solar wind protons took place in the magnetosheath before reaching the magnetic barrier.

The elapsed time between the inbound and outbound ICB crossings decreased on the day when the ICME arrived. The analysis of the dayside altitude of the ICB showed that it was not affected by the ICME. The position of the ICB at the nightside was found closer to the planet which explains why VEX spent less time in the ionosphere. Our analysis of the ionosphere showed that one of the most significant differences between the response of the Venusian and Martian ionospheres is that the Martian ionosphere extended at the nightside during the passage of the ICME sheath region [*Morgan et al*., 2014], while at Venus, it was observed that the nightside ionosphere decreased.

7. Conclusions

We have studied the induced magnetosphere of Venus when the magnetic field magnitude of the magnetic barrier was anomalously large due to ICME passages. We found that these ICMEs can be characterized with increased tangential magnetic field component and interplanetary shocks. We conclude that these two features have the most significant effect on the observed high magnetic field intensities of the magnetic barrier.

The effects of the ICME sheath region and the magnetic cloud on the bow shock were distinguished from each other. Anomalously large bow shock crossings occurred only during magnetic cloud passages. This is explained by the decreased magnetosonic Mach number during those periods. During the ICME sheath region passage the position of the bow shock remained unchanged.

The positions of the upper and lower boundaries of the magnetic barrier were not affected by the ICMEs. We conclude that the anomalously large magnetic field intensities are not related to the shrinking of the altitude of the magnetic barrier. We suggest that the anomalously large magnetic field is rather the result of the very intense magnetic field in the ICME sheath region which suddenly piles up in front of the obstacle.

We found that the variation of the position of the Venusian ionosphere at the dayside remains quite unchanged during the extreme space weather conditions. The nightside ionosphere and the altitude of the ICB decreased during the passage of the ICME sheath region which can be explained by the fact that the ion loss into the interplanetary space must have increased due to the enhanced dynamic pressure associated with the arrival of the interplanetary shock.

Acknowledgments

Data were sourced from the European Space Agency's Planetary Science Archive (www.rssd.esa.int/PSA). Part of the data analysis was done with the AMDA (http://amda.cdpp.eu/) science analysis system provided by the Centre de Données de la Physique des Plasmas (IRAP, Université Paul Sabatier, Toulouse) supported by CNRS and CNES. The authors thank the VEX ASPERA-4 and MAG teams for making their data available in the PSA and AMDA systems. The authors also thank the STEREO and SOHO teams for providing their data (http://stereo.nascom.nasa.gov/cgi-bin/images and http://sohodata.nascom.nasa.gov/cgi-bin/data_query). The authors are also grateful for the assistance of Lan Jian (NASA GSFC Heliophysics Science Division) and Benjamin Hawe (Luleå University of Technology). Andrea Opitz is currently a research fellow at ESA/ESTEC. Daniel Vech acknowledges support from the Science Faculty to visit ESA/ESTEC for the collaboration.

Yuming Wang thanks the reviewers for their assistance in evaluating this paper.

References

Alexander, J. C., and C. T. Russel (1985), Solar cycle dependence of the location of the Venus bow shock, *Geophys. Res. Lett.*, *12*, 369–371.

Angsmann, A., M. Fränz, E. Dubinin, J. Woch, S. Barabash, T. Zhang, and U. Motschmann (2011), Magnetic states of the ionosphere of Venus observed by Venus Express, *Planet. Space Sci.*, *59*, 327–337, doi:10.1016/j.pss.2010.12.004.

Barabash, S., et al. (2007), The Analyzer of Space Plasmas and Energetic Atoms (ASPERA-4) for the Venus Express mission, *Planet. Space Sci.*, *55*, 1772–1792, doi:10.1016/j.pss.2007.01.014.

Burlaga, L., E. Sittler, F. Mariani, and R. Schwenn (1981), Magnetic loop behind an interplanetary shock: Voyager, Helios and IMP 8 observations, *J. Geophys. Res.*, *86*, 6673–6684.

Chai, L., M. Fraenz, W. Wan, Z. Rong, T. Zhang, Y. Wei, E. Dubinin, J. Zhong, X. Han, and S. Barabash (2014), IMF control of the location of Venusian bow shock: The effect of the magnitude of IMF component tangential to the bow shock surface, *J. Geophys. Res. Space Physics*, *119*, 9464–9475, doi:10.1002/2014JA019878.

Domingo, V., and A. Poland (1988), The SOHO project: Helioseismology investigations, *Adv. Space Res.*, *8*(11), 109–115.

Edberg, N. J. T., M. Lester, S. W. H. Cowley, D. A. Brain, M. Fränz, and S. Barabash (2010), Magnetosonic Mach number effect of the position of the bow shock at Mars in comparison to Venus, *J. Geophys. Res.*, *115*, A07203, doi:10.1029/2009JA014998.

Edberg, N. J. T., et al. (2011), Atmospheric erosion of Venus during stormy space weather, *J. Geophys. Res.*, *116*, A09308, doi:10.1029/2011JA016749.

Farris, M. H., and C. T. Russell (1994), Determining the standoff distance of the bow shock: Mach number dependence and use of models, *J. Geophys. Res.*, *99*, 17,681–17,689.

Fedorov, A., et al. (2008), Comparative analysis of Venus and Mars magnetotails, *Planet. Space Sci.*, *56*, 812–817, doi:10.1016/j.pss.2007.12.012.

Fraenz, M., E. Dubinin, E. Roussos, J. Woch, J. D. Winningham, R. Frahm, A. J. Coates, A. Fedorov, S. Barabash, and R. Lundin (2006), Plasma moments in the environment of Mars: Mars Express ASPERA-3 observations, *Space Sci. Rev.*, *126*, 165–207, doi:10.1007/s11214-006-9115-9.

Gosling, J. T. (1990), Coronal mass ejections and magnetic flux ropes in interplanetary space, in *Physics of Magnetic Flux Ropes*, *Geophys. Monogr.*, vol. 58, edited by E. R. Priest, L. C. Lee, and C. T. Russell, pp. 343–364, AGU, Washington, D. C.

Jian, L., C. T. Russel, J. G. Luhmann, A. B. Galvin, and K. D. C. Simunac (2013), Solar wind observations at STEREO: 2007–2011, AIP Conf. Proc. 1539, 191, doi:10.1063/1.4811020.

Kaiser, M. L., T. A. Kucera, J. M. Davila, S. O. C. Cyr, M. Guhathakurta, and E. Christian (2008), The STEREO mission: An introduction, *Space Sci. Rev.*, *136*, 5–16, doi:10.1007/s11214-007-9277-0.

Kilpua, E. K. J., A. Isavnin, A. Vourlidas, H. E. J. Koskinen, and L. Rodriguez (2013), On the relationship between interplanetary coronal mass ejections and magnetic clouds, *Ann. Geophys.*, *31*, 1251–1265, doi:10.5194/angeo-31-1251-2013.

Leamon, R. J., R. C. Canfield, and A. A. Pevtsov (2002), Properties of magnetic clouds and geomagnetic storms associated with eruption of coronal sigmoids, *J. Geophys. Res.*, *107*(A9), 1234, doi:10.1029/2001JA000313.

Lepping, R. P., C.-C. Wu, and D. B. Berdichevsky (2005), Automatic identification of magnetic clouds and cloud-like regions at 1 AU: Occurrence rate and other properties, *Ann. Geophys.*, *23*, 2687–2704.

Luhmann, J. G., A. Fedorov, S. Barabash, E. Carlsson, Y. Futaana, T. L. Zhang, C. T. Russell, J. G. Lyon, S. A. Ledvina, and D. A. Brain (2008), Venus Express observations of atmospheric oxygen escape during the passage of several coronal mass ejections, *J. Geophys. Res.*, *113*, E00B04, doi:10.1029/2008JE003092.

Martinecz, C., et al. (2008), Location of the bow shock and ion composition boundaries at Venus—Initial determinations from Venus Express ASPERA-4, *Planet. Space Sci.*, *56*, 780–784, doi:10.1016/j.pss.2007.07.007.

Martinecz, C., et al. (2009), Plasma environment of Venus: Comparison of Venus Express ASPERA-4 measurements with 3-D hybrid simulations, *J. Geophys. Res.*, *114*, E00B30, doi:10.1029/2008JE003174.

McEnulty, T. R., J. G. Luhmann, I. de Pater, D. A. Brain, A. Fedorov, T. L. Zhang, and E. Dubinin (2010), Interplanetary coronal mass ejection influence on high energy pick-up ions at Venus, *Planet. Space Sci.*, *58*, 1784–1791, doi:10.1016/j.pss.2010.07.019.

Morgan, D. D., et al. (2014), Effects of a strong ICME on the Martian ionosphere as detected by Mars Express and Mars Odyssey, *J. Geophys. Res. Space Physics*, *119*, 5891–5908, doi:10.1002/2013JA019522.

Russell, C. T., and T. L. Zhang (1992), Unusually distant bow shock encounters at Venus, *Geophys. Res. Lett.*, *19*, 833–836, doi:10.1029/92GL00634.

Russell, C. T., E. Chou, J. G. Luhmann, P. Gazis, L. H. Brace, and W. R. Hoegy (1988), Solar and interplanetary control of the location of the Venus bow shock, *J. Geophys. Res.*, *93*(A6), 5461–5469, doi:10.1029/JA093iA06p05461.

Russell, C. T., J. G. Luhmann, and R. J. Strangeway (2006), The solar wind interaction with Venus through the eyes of the Pioneer Venus Orbiter, *Planet. Space Sci.*, *54*, 1482–1495, doi:10.1016/j.pss.2006.04.025.

Slavin, J. A., R. C. Elphic, and C. T. Russel (1979), A comparison of Pioneer Venus and Venera bow shock observations: Evidence for a solar cycle variation, *Geophys. Res. Lett.*, *6*, 905–908.

Svedhem, H. (2014), Aerobraking with Venus Express, *ESA Bull.-Eur. Space Agency*, *159*, 43–46.

Svedhem, H., et al. (2007), Venus Express—The first European mission to Venus, *Planet. Space Sci.*, *55*, 1636–1652, doi:10.1016/j.pss.2007.01.013.
Titov, D. V., et al. (2006), Venus Express science planning, *Planet. Space Sci.*, *54*, 1279–1297, doi:10.1016/j.pss.2006.04.017.
Wei, Y., et al. (2012), A teardrop-shaped ionosphere at Venus in tenuous solar wind, *Planet. Space Sci.*, *73*, 254–261, doi:10.1016/j.pss.2012.08.024.
Zhang, T. L., J. G. Luhmann, and C. T. Russell (1991), The magnetic barrier at Venus, *J. Geophys. Res.*, *96*(A7), 11,145–11,153, doi:10.1029/91JA00088.
Zhang, T. L., K. K. Khurana, C. T. Russel, M. G. Kivelson, R. Nakamura, and W. Baumjohann (2004), On the Venus bow shock compressibility, *Adv. Space Res.*, *33*, 1920–1923, doi:10.1016/j.asr.2003.05.038.
Zhang, T. L., et al. (2006), Magnetic field investigation of the Venus plasma environment: Expected new results from Venus Express, *Planet. Space Sci.*, *54*, 1336–1343, doi:10.1016/j.pss.2006.04.018.
Zhang, T. L., et al. (2008a), Initial Venus Express magnetic field observations of the magnetic barrier at solar minimum, *Planet. Space Sci.*, *56*, 790–795, doi:10.1016/j.pss.2007.10.013.
Zhang, T. L., et al. (2008b), Venus Express observations of an atypically distant bow shock during the passage of an interplanetary coronal mass ejection, *J. Geophys. Res.*, *113*, E00B12, doi:10.1029/2008JE003128.
Zhang, T. L., J. Du, Y. J. Ma, H. Lammer, W. Baumjohann, C. Wang, and C. T. Russell (2009), Disappearing induced magnetosphere at Venus: Implications for close-in exoplanets, *Geophys. Res. Lett.*, *36*, L20203, doi:10.1029/2009GL040515.